OPEN

NPG Asia Materials (2015) 7, e201; doi:10.1038/am.2015.74

www.nature.com/am

ORIGINAL ARTICLE

Combining the lotus leaf effect with artificial photosynthesis: regeneration of underwater superhydrophobicity of hierarchical ZnO/Si surfaces by solar water splitting

Junghan Lee and Kijung Yong

Fabrication of stable superhydrophobic surfaces in dynamic circumstances is a key issue for practical uses of non-wetting surfaces. However, superhydrophobic surfaces have finite lifetime in underwater conditions due to the diffusion of gas pockets into the water. To overcome this limited lifetime of underwater superhydrophobicity, this study introduces a novel method for regenerating a continuous air interlayer on superhydrophobic ZnO nanorod/Si micropost hierarchical structures (HRs) via the combination of two biomimetic properties of natural leaf: superhydrophobicity from the lotus leaf effect and solar water splitting from photosynthesis. The designed n/p junction in the ZnO/Si HRs allowed for highly stable gas interlayer in water and regeneration of the underwater superhydrophobicity due to the unique ability of the surface to capture and retain a stable gas layer. Furthermore, we developed a model to determine the optimum structural factors of hierarchical ZnO/Si surfaces that aid the formation of an air interlayer to completely regenerate the superhydrophobicity. We also verified that this model satisfactorily predicted the regeneration of underwater superhydrophobicity under various experimental conditions. The regenerative method developed in this work is expected to broaden the range of potential applications involving superhydrophobic surfaces and to create new opportunities for related technologies.
NPG Asia Materials (2015) **7,** e201; doi:10.1038/am.2015.74; published online 17 July 2015

INTRODUCTION

Superhydrophobic surfaces that mimic lotus leaves have been extensively studied over the past several decades, and various micro/nanostructures have been developed to create bio-inspired superhydrophobic surfaces.[1–15] In recent years, the non-wetting property of superhydrophobic surfaces submerged in water has attracted much attention because it has potential applications in drag reduction, anti-fouling, anti-corrosion, waterproof devices, microchannels, anti-icing and other non-wetting related applications.[16–25] Practical applications of non-wetting surfaces, however, have been impeded by the limited stability of their underwater superhydrophobicity.[26–28] According to the Cassie–Baxter model, the presence of an air interlayer on the submerged surface causes the non-wetting behavior, and thus, the stability of underwater superhydrophobicity is determined by the lifetime of the air (or gas) interlayer captured by the superhydrophobic surface.[29] However, the gas interlayer is unstable due to diffusion of the gas into the water.[30] According to previous studies, the gas diffusion rates are strongly affected by physical (hydrostatic pressure and micro/nanostructures of the surface) and chemical (surface energy) factors.[26,31]

Although several investigations have been performed to understand the mechanism controlling the stability of the underwater non-wetting property, few studies have explored regenerating a stable gas interlayer to restore the underwater superhydrophobicity.[32] Up to now, superhydrophobic surfaces have only been shown to repair or reconstruct themselves via thermal or photochemical post-treatments under atmospheric conditions that restore their surface structures.[33–36] To regenerate underwater superhydrophobicity, it is essential to develop a method for producing gas and restoring the gas layer on the surface. A smart way to generate gases underwater is to use the water contacting the surface; for example, photocatalytic water splitting can be employed to regenerate the surface gas layer. Solar water splitting is an artificial leaf effect that mimics photosynthesis in natural leaves.[37] In recent years, water-splitting technologies for hydrogen gas generation have been explored globally to develop future alternative energy sources.[38,39]

This study presents the first attempt to combine two biomimetic properties of natural leaves, the lotus leaf effect (superhydrophobicity) and artificial leaf effect (photosynthesis), and aims to use hydrogen gas generated by solar water splitting to restore a continuous gas interlayer on submerged superhydrophobic surfaces (Scheme 1). A crucial factor

Department of Chemical Engineering, Surface Chemistry Laboratory of Electronic Materials, POSTECH (Pohang University of Science and Technology), Pohang, Korea
Correspondence: Professor K Yong, Department of Chemical Engineering, Surface Chemistry Laboratory of Electronic Materials, POSTECH (Pohang University of Science and Technology), San 31, Hyoja-dong, Nam-gu, Pohang, Kyungbuk 790-784, Korea.
E-mail: kyong@postech.ac.kr
Received 31 January 2015; revised 18 March 2015; accepted 27 April 2015

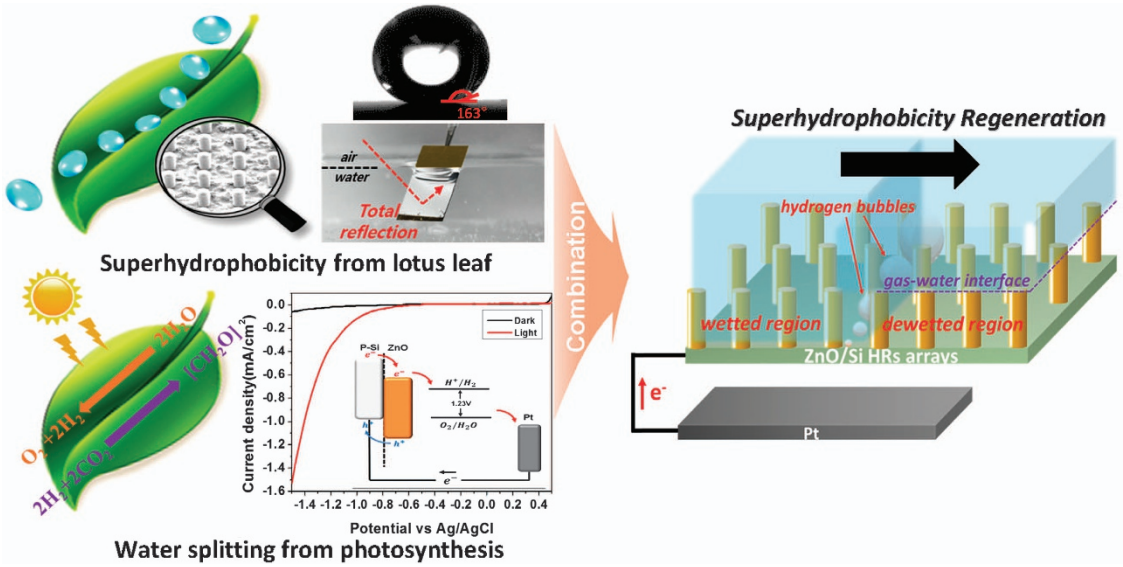

Scheme 1 An illustration of underwater superhydrophobicity regeneration system.

for realizing this objective is to fabricate photocatalytic nanomaterials with low surface energies that act as both the micro-/nano-sized hierarchical papillae in lotus leaves and the photoelectrode for photosynthetic hydrogen generation in artificial leaves. Furthermore, an optimal superhydrophobic surface structure is required to efficiently capture and retain the evolved gas because the ability of the surface to retain the underwater gas layer is intimately related to its morphology.

We fabricated and tested various micro/nanostructures to study the stability and regeneration of underwater superhydrophobicity. To systematically investigate structural effects, three samples were prepared: ZnO nanorods (NRs), Si microposts (MPs) and ZnO/Si hierarchical structures (HRs) combining ZnO NRs and Si MPs. First, the stability of the underwater superhydrophobicity of each sample was investigated by measuring the lifetime of the gas interlayer (plastron). Then, the experimental results for hydrogen gas generation by solar water splitting at the surface were used to propose a theoretical model to determine the prerequisite geometric criteria for capturing gas bubbles and forming stable gas interlayers to completely regenerate the underwater superhydrophobicity. Of the samples investigated, the ZnO/Si HRs most successfully satisfied the requirements for high stability and complete regeneration of the underwater superhydrophobicity. A theoretical model was also developed to define the optimum hierarchical ZnO/Si surface structure for regenerating a stable gas interlayer underwater. The regeneration method developed in this study will broaden the range of potential applications involving superhydrophobic surfaces and create new opportunities for related technologies.

EXPERIMENTAL PROCEDURE

ZnO NRs growth

ZnO NRs of diverse length were synthesized using a simple hydrothermal method. A 50-nm-thick ZnO thin seed film was deposited on an Fluorine doped Tin Oxide (FTO) glass by radio frequency magnetron sputtering using a ZnO target under 8.0×10^3 torr Ar atmosphere at room temperature. The sputtered seed film was immersed in an aqueous solution containing 0.01 M $ZnO(NO_3)_2 \bullet 6H_2O$ (98%, Sigma-Aldrich, Seoul, Korea) and 0.2 M NH_4OH (28 wt% NH_3 in water, 99.99%, Sigma-Aldrich) for 6 h at 95 °C. After the NR growth, the substrates were rinsed with deionized water and ethanol, and then dried with N_2 gas.

Fabrication of ZnO/Si HRs structure

For a fabrication of the MPs with varying diameters of the post and pitches between the posts, photolithography method was used. A 50-μm-thick negative photoresist (KMPR1050, Microchem, Gyeonggi-do, Korea) was spin coated on p-type silicon wafer and prebake process was conducted to evaporate the coating solvent and to densify the resist after spin coating. A Cr photomask was deposited on the substrate, and photoetching was conducted with uniform ultraviolet exposure illumination. Then remained photoresists were removed by acetone and trichloroethylene. MPs with varying diameters and pitches were patterned out of the photoresist. ZnO NRs were uniformly grown on the as-synthesized Si MPs by the hydrothermal method. The details of method were same as above ZnO NRs growth section.

Wettability control

Teflon AF solution (polytetrafluoroethylene (PTFE), Teflon Amorphous Fluoro-polymer 1600; copolymers of tetraflouroethlene, purchased from DuPont, Seoul, Korea) was spin coated on the as-prepared substrates by 5 times at 2000 rpm, 30 s. The films were heated up to 60 °C for 30 min to obtain fully heat-cured PTFE. The water contact angle measurements were conducted to verify successful deposition of PTFE on the substrates

Analysis of underwater superhydrophobic stability

The stability test of underwater superhydrophobicity was performed with each micro/nanostructure at varying immersion depths. The superhydrophobic surfaces were laid in the glass water tank, tilted at 45°. The video camera was installed at the optimized position to record the images of submerged superhydrophobic surfaces during the experiments. The stability times of underwater superhydrophobicity of ZnO NRs surfaces, Si MPs surfaces and ZnO/Si HRs surfaces were measured by altering the sample immersion depth. The stability times were measured when the water depth was 5, 10, 15 and 20 cm respectively. The recorded images were converted to gray mode, and a threshold was applied. The threshold value was fixed at 225 for entire images. The numbers of white and black pixels were measured, and the plastron intensity was defined as the ratio of white pixels to entire pixels. Then the plastron intensity data were plotted by time.

Photoelectrochemical reaction

The photocurrent–voltage (*I–V*) measurements were performed by a three potentiostat system (potentiostat/galvanostat, model 263A, EG&G Princeton Applied Research, Gyeonggi-do, Korea) with a Pt mesh as counter electrode and a saturated calomel reference electrode. The as-prepared ZnO/Si HRs substrates were used as working electrode and a 0.4 M Na_2SO_4 aqueous solution with nitrogen purged was used for electrolyte. The working electrode was illuminated with a solar-simulated light source (AM 1.5 G filtered, 100 mW cm^{-2}, 9ll60, Oriel, Daejeon, Korea) and then the *I–V* curve was measured.

Electrolysis

The as-prepared ZnO NRs substrate and Si MPs substrates were used as working electrode, Pt mesh was used as a counter electrode and a 1 M NaCl aqueous solution with nitrogen purging was used for electrolyte. For electrolysis, we applied 4 V between the working and counter electrode using power supply.

Characterization

The morphology, structure and composition of the as-synthesized HRs were examined using field emission scanning electron microscopy (JEOL, Model JSM 330F). The water contact angles were measured by contact angle measurement system (Krűss, Model DSA-10, Hamburg, Germany) with 5 μl deionized water. The states of sample submerged underwater were recorded by a web-camera (@info, ALC-M1000).The underwater superhydrophobicity regeneration processes were recorded by optical microscopy (JENOPTIK ProgRes MF, Gyeonggi-do, Korea).

RESULTS AND DISCUSSION

Fabrication and wettability control of ZnO NRs, Si MPs and ZnO/Si HRs

First, highly uniform ZnO NRs were synthesized by a simple hydrothermal method.[40] After the reaction, a dense layer of ZnO NRs was vertically grown on the substrate (Figure 1a). As shown in Figures 1a–c, the as-synthesized ZnO NRs had a high aspect ratio with lengths of 8–10 μm, diameters of ~50 nm and spacings of a few hundred nanometers. The length of the ZnO NRs was facilely controlled by varying the pH of the aqueous solution or the ammonium hydroxide concentration. The second sample consisting of Si MPs was fabricated by a typical photolithography method.[41] The Si MPs had a height of ~50 μm and diameter of ~20 μm, and the pitch between the posts was ~100 μm, as shown in Figures 1d–f. Si MPs with different pitch spacings (30 and 50 μm) were also fabricated using the appropriate Cr photomasks. The third sample consisted of ZnO NR/Si MP HRs that were fabricated by combining the above two synthesis procedures. After synthesizing the ZnO NRs on the Si MPs, a highly uniform and dense growth of ~8 μm ZnO NRs covered the entire Si MP surface (Figures 1g–i). ZnO/Si HRs with longer ZnO NRs (~17 μm) were also synthesized by repeating the ZnO NR synthesis two times (Figures 1j–l), which resulted in a more sharply defined and dense growth of ZnO NRs on the Si MPs. ZnO/Si HRs with different MP pitch spacings (30 and 50 μm) were also fabricated (Supplementary Figure S1).

The water contact angles (CAs) of the as-grown ZnO NR and ZnO/Si HR surfaces were below 5°, which indicated superhydrophilic

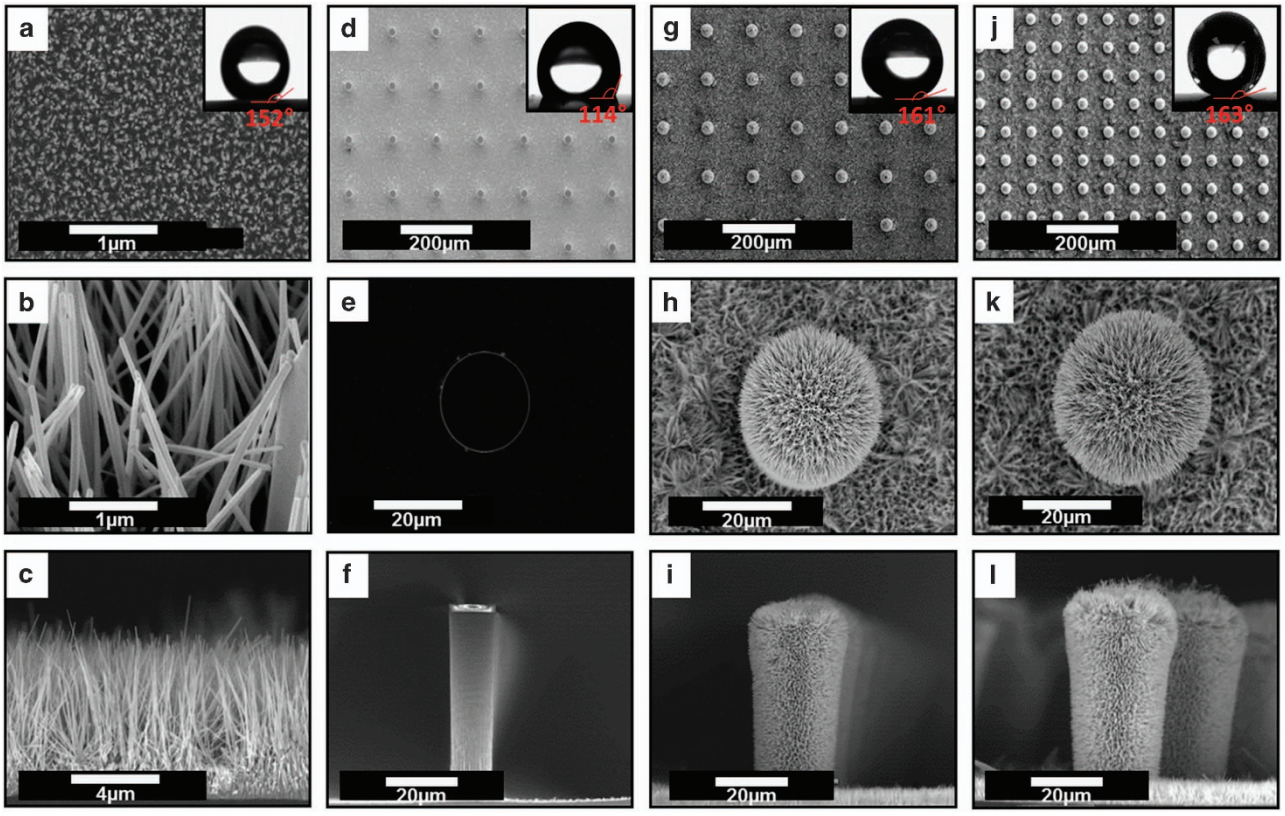

Figure 1 Field emission scanning electron microscopy top, magnified and cross-sectional images of (**a**–**c**) ZnO NRs, (**d**–**f**) Si MPs and (**g**–**i**) ZnO/Si HRs with a 100-μm micropost spacing, and (**j**–**l**) ZnO/Si HRs with a 50-μm micropost spacing. The inset images in **a**, **d**, **g** and **j** show the static water contact angles of PTFE-coated ZnO NRs, Si MPs and ZnO/Si HRs with a 100-μm micropost spacing, and ZnO/Si HRs with a 50-μm micropost spacing, respectively.

wettability due to the –OH functional groups on the hydrothermally grown ZnO NR surface.[42] The bare Si MPs exhibited moderate hydrophilic wettability with water CAs of ~ 50°. To reduce the surface energy and render the surfaces superhydrophobic, a Teflon AF solution (PTFE) was spin coated on the samples.[43] Because of the PTFE C–F chains, the PTFE-modified surfaces exhibited hydrophobicity. The static water CAs of the ZnO NRs, 100-μm pitch Si MPs, ZnO/Si HR sample **A** (8-μm long NRs/100-μm pitch MPs) and ZnO/Si HR sample **B** (17-μm long NRs/50-μm pitch MPs) were 152°, 114°, 161° and 163°, respectively, as depicted in the inset images in Figures 1a, d, g and j, respectively (more SEM images, transition graph of water CAs and Fourier transform infrared spectrum for the samples before and after PTFE coating were described in Supplementary Information 1,2 and 3). The differences in the static water CAs of the samples were due to differences in the surface roughness. According to the Cassie–Baxter equation, $\cos\theta^* = rf\cos\theta_Y + f - 1$, (where θ^* is the static CA, r is the surface roughness, f is the solid surface area fraction and θ_Y is the Wenzel CA), the static water CAs are strongly affected by the surface roughness r. Consequently, the Si MPs with a relatively low surface roughness exhibited moderate hydrophobicity with a CA of 114°. By contrast, the ZnO NR surface exhibited superhydrophobicity with a CA of 152° because it had a higher surface roughness, and the ZnO/Si HR samples, which had the highest surface roughness, had the highest water CAs of 161° and 163°.

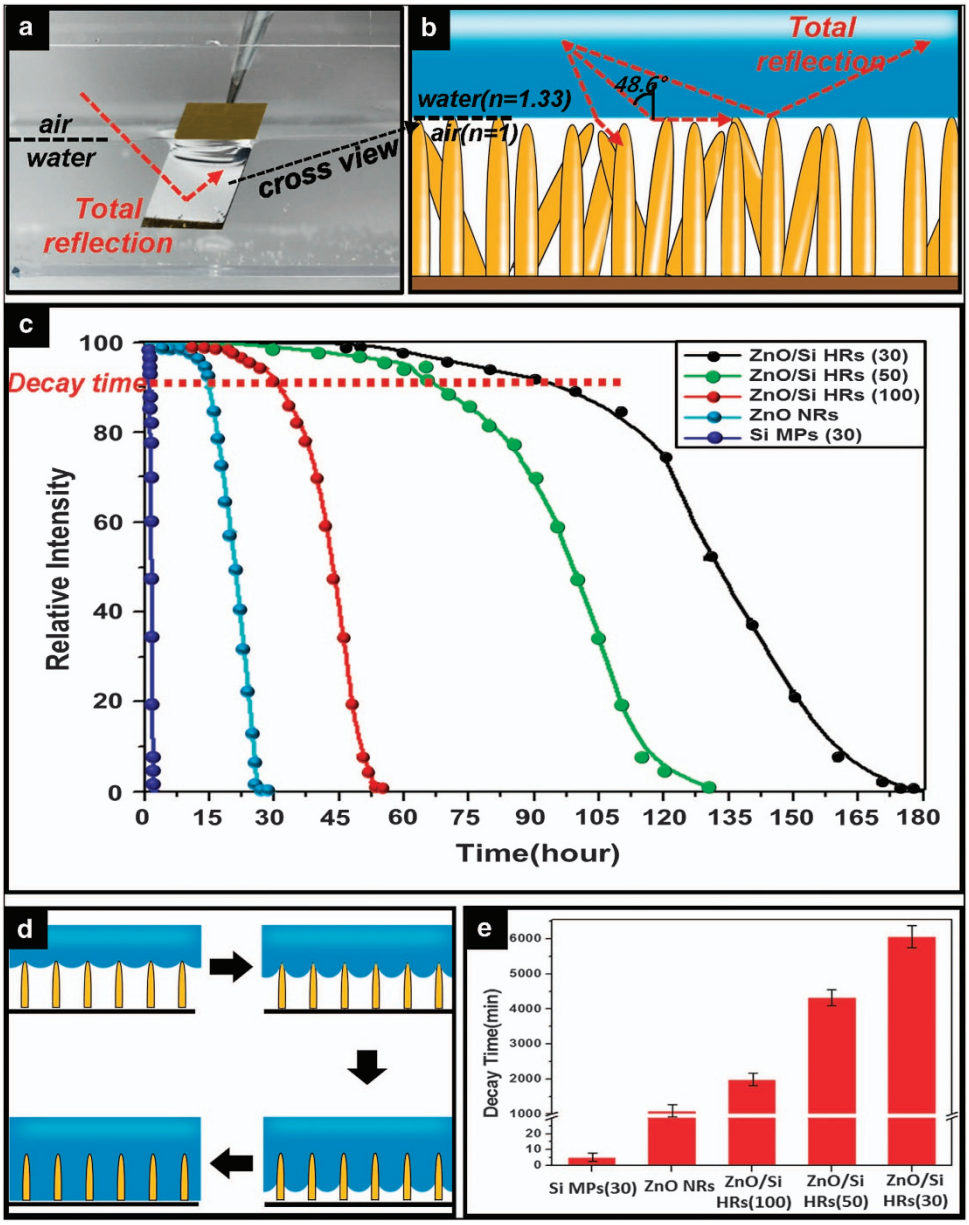

Figure 2 (**a**) Digital image of superhydrophobic ZnO NRs submerged in water. The submerged part of the substrate had a silvery surface due to total light reflection at the water–air interface. (**b**) Schematic images describing the total reflections at the water–air interface. (**c**) Relative intensity transitions of the Si MPs with a 30-μm micropost spacing, ZnO NRs and ZnO/Si HRs with 100, 50 and 30-μm micropost spacings when submerged in water at a depth of 20 cm. The relative intensity represents the stability of the underwater superhydrophobicity. (**d**) Schematic images demonstrating the mechanism by which the submerged substrate loses its underwater superhydrophobicity. (**e**) Decay time (τ_d) for the submerged substrates.

Stability analysis of underwater superhydrophobic ZnO NRs, Si MPs and ZnO/Si HRs

When the as-synthesized ZnO NRs, Si MPs and ZnO/Si HRs were submerged in water, the vivid change in visual aspect was found on the surface (Figure 2a).[44] The ZnO NRs and ZnO/Si HRs were initially yellow and dark gray, respectively, in air but exhibited mirror-like silvery surfaces in water. This phenomenon occurred because the presence of the air interlayer between the micro/nanostructures and the water interface reflected all light (total reflection effects) (Figure 2b). When light travels from a medium with a higher refractive index (the water layer; refractive index of 1.33) to a lower refractive index medium (the air pocket; refractive index of 1), all incident lights that strike the surface at an angle greater than a certain critical angle ($\theta_c = 48°$ for the water/air interface) are reflected.[31]

The effects of the surface structure on the stability of the underwater superhydrophobicity were investigated by measuring the plastron (gas layer) lifetimes for three different ZnO NR, Si MP and ZnO/Si HR samples. Specifically, the optical changes in the mirror-like surface were analyzed with a webcam. The optical image of the submerged superhydrophobic surface initially consisted of bright pixels due to mirror-like total reflection but the pixels became dark when the gas in the plastron began to diffuse into the water. Plotting the ratio of bright pixels to dark pixels allowed the superhydrophobicity lifetimes to be quantified.[26]

The relative bright pixel intensities representing the gas interlayer stability were plotted as a function of the immersion time for the ZnO NR, Si MP (30-μm pitch) and ZnO/Si HR samples (30-, 50- and 100-μm pitches) (Figure 2c). The immersion depth of the substrates was 20 cm. As shown in Figure 2c, regardless of the surface morphology, the maximum plastron intensities were observed at the beginning of the experiment for all the samples, and after a certain time, the intensities decreased rapidly. All of the surfaces became completely wetted, indicating that the superhydrophobicity was lost. To analyze the decay of the superhydrophobicity quantitatively for the different sample types, the decay time (τ_d), which was defined as the time at which the ratio of bright pixels to dark pixels reached 90%, was measured (Figure 2e). The relative plastron intensities of the substrates decreased sharply after τ_d. The 30-μm-pitch Si MP sample exhibited stable underwater superhydrophobicity with a short τ_d of 5 min. By contrast, the 50- and 100-μm-pitch Si MP samples were completely wetted within seconds of being submerged in water. The stability of the ZnO NR superhydrophobicity was much higher, as demonstrated by a τ_d of 1080 min. The ZnO NR/Si MP combined hierarchical samples had much longer decay times of 6060, 4320 and 1980 min for the 30-, 50- and 100-μm-pitch MPs, respectively, with 8-μm-long ZnO NRs. These results indicate that the multi-scale micro/nanostructures of the hierarchical samples are highly effective at retaining the air interlayer in water.[45] Longer τ_d values were observed for the narrower pitches due to the Laplace pressure (p_L) induced by the capillary force, $p_L = 2\gamma\cos\theta_0/d$ (where γ is the water surface tension, θ_0 is the water CA on the flat surface and d is the pitch), which inhibited water diffusion into the structure. According to the Laplace pressure equation, the capillary force increases as the pitch becomes narrower. The out-diffusion process of the air interlayer in water is depicted in Figure 2d.

In addition, we have tested the effect of coating material on the underwater superhydrophobicity by applying stearic acid instead of PTFE. Our results showed that two coating materials showed similiar stability time and tendency (Supplementary Information 4).

Regeneration of underwater superhydrophobicity by photoelectrochemical reaction

After the loss of the air interlayer, the water at the micro/nanostructure surface can be used to generate hydrogen gas by photoelectrochemical (PEC) water splitting. Figure 3a shows the PEC current generation results for the PEC system with a ZnO/Si HR photocathode as the working electrode.[46] All the measurements were performed in a three-electrode PEC system with a Pt wire and saturated calomel electrode as the counter and reference electrodes, respectively. A 0.4 M Na_2SO_4 aqueous solution was used as the electrolyte. The measured potential *vs* reversible hydrogen electrode was obtained using the Nernst equation. The current density–potential (*J*–*V*) results indicate that the ZnO/Si HR electrode generated a high photocurrent under 1 Sun, AM 1.5 G illumination. Because p-type Si MPs were used as the electrode in this study, cathodic current generation occurred. In this system, electrons photogenerated at the working electrode reduced H^+ ions to generate hydrogen gas at the photocathode, and water was

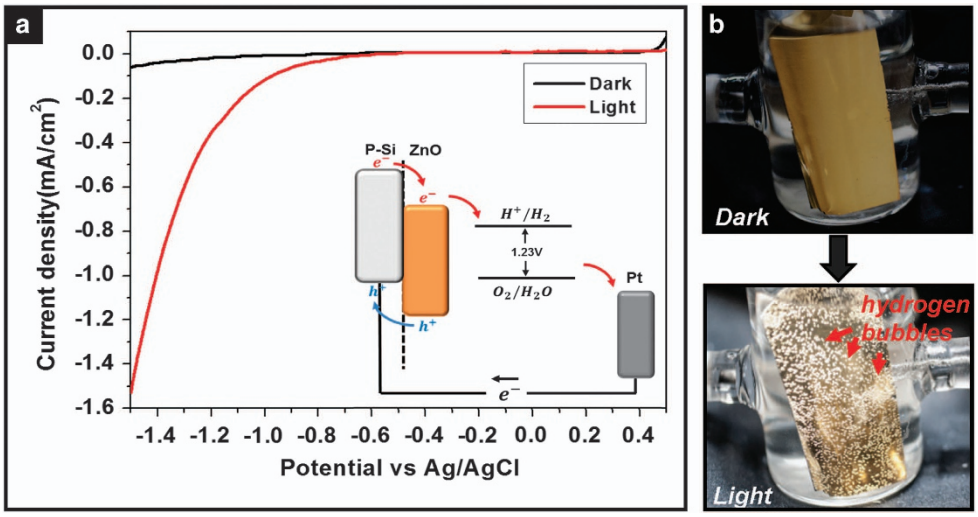

Figure 3 (**a**) Photocurrent density vs applied potential in the dark and light. The inset image shows the proposed energy gap structure for the hydrogen generation process. (**b**) Digital images demonstrating the generation of hydrogen gas bubbles in the dark and light.

oxidized at the counter electrode (Pt). N-type ZnO NRs grown on the p-type Si MPs led to the creation of p–n junctions, which resulted in enhanced light absorption and efficient charge separation.[46] The inset image in Figure 3a shows a schematic energy band diagram for the ZnO/Si HR PEC system. When a high reverse bias was induced, significant band bending occurred at the p-type Si and n-type ZnO NR junction. This band bending resulted in a reduced barrier between the n-type ZnO NRs and the electrolyte, leading to a large photocathodic current and hydrogen generation. Figure 3b shows the generation of gas bubbles on the ZnO/Si HRs in the dark and light. In the dark, gas bubbles were not generated due to the absence of a photon source. In contrast, exposure to light resulted in the evolution of numerous gas bubbles on the surfaces. The photocurrent generation can be further enhanced by applying co-catalysts such as Pt. Pt layer deposited ZnO/Si HRs showed generation of higher photocurrent density. (more details are presented in Supplementary Information 5). The PEC photocurrents of the ZnO NRs and Si MPs were too low to generate enough hydrogen gas. Thus, water electrolysis was used instead of the PEC reaction to generate gas bubbles on the ZnO NR and Si MP surfaces.

The photoelectrochemically generated hydrogen gas was used to regenerate the gas layer and underwater superhydrophobicity. However, the effectiveness of the regeneration strongly depended on the ability of the surface structure to capture and retain the gas. The

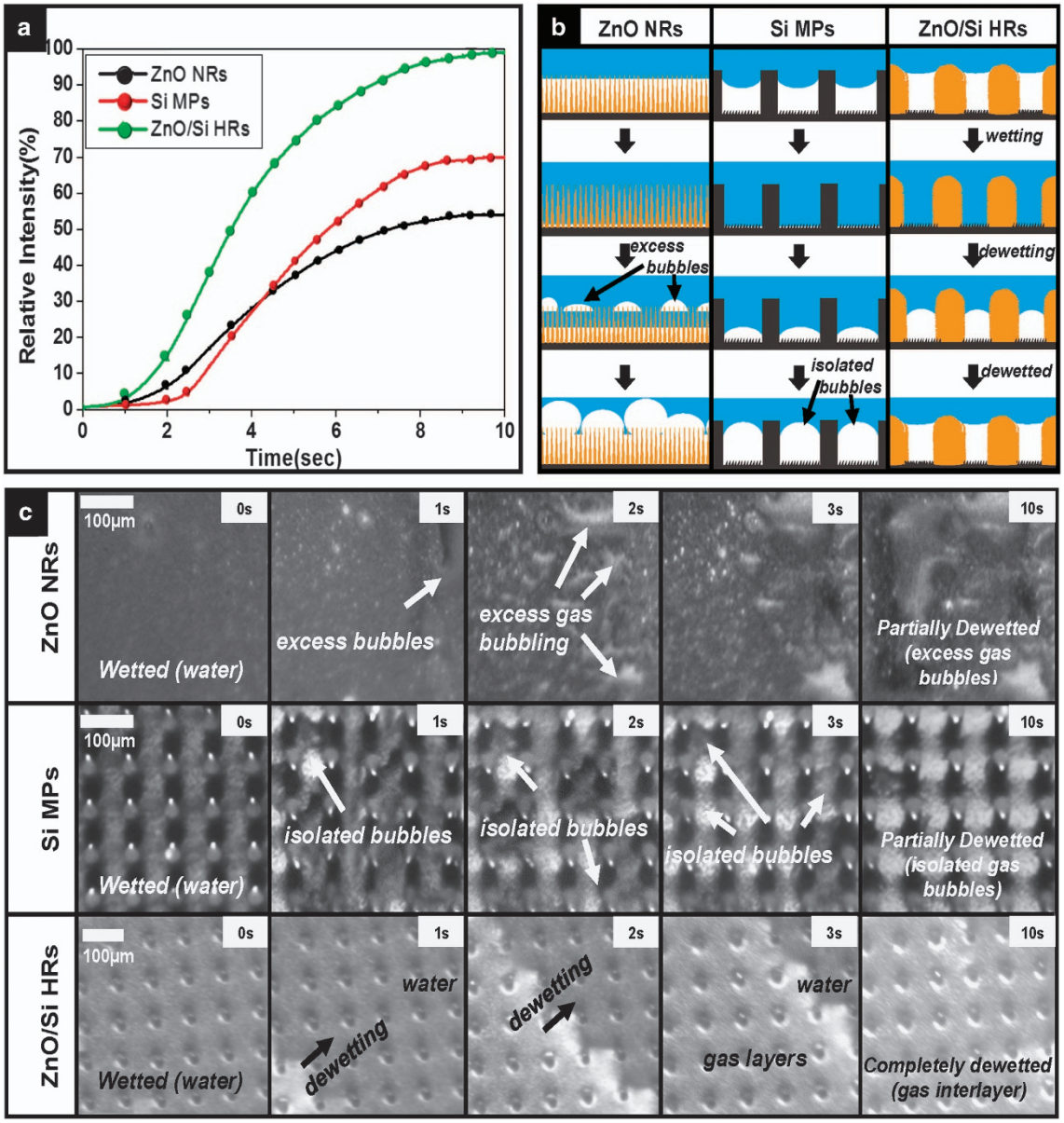

Figure 4 (**a**) Relative intensity transitions of the ZnO NRs, Si MPs and ZnO/Si HRs during superhydrophobicity regeneration by underwater gas generation. (**b**) Schematic images of the wetting and dewetting processes of the superhydrophobic ZnO NRs, Si MPs and ZnO/Si HRs. The underwater superhydrophobicity of the ZnO NRs was not completely restored due to the narrow spacing between them. The underwater superhydrophobicity of the Si MPs was not completely regenerated due to the formation of isolated gas bubbles between the microposts. The underwater superhydrophobicity of the ZnO/Si HRs was completely regenerated. (**c**) Microscope images showing the regeneration of gas bubbles on the ZnO NRs, Si MPs and ZnO/Si HRs.

regeneration characteristics were investigated using three samples of the ZnO NRs, Si MPs and ZnO/Si HRs, and the results are compared in Figure 4. The relative bright pixel intensities of the three samples increased similarly over time during the PEC or electrolysis reaction, but the maximum intensities differed considerably.

The relative intensity of the ZnO NRs increased rapidly for 5 s. Then, the rate of increase slowed gradually, and the relative intensity plateaued at only 54% of the maximum value 10 s after the gas generation was initiated Figure 4a. The superhydrophobicity was only partially regenerated due to excess gas bubbles on the top of the ZnO NRs as observed in the microscopy images in Figure 4c. When the reaction began, gas bubbles started to evolve on the ZnO NR surface. On the basis of the analysis of the gas bubble formation and diffusion in water, the minimum diameter required to sustain a gas bubble in the water was ~ 20 μm.[47,48] For the ZnO NRs, the spacing between the NRs was too small for the gas bubbles to fit between the NRs (the spacing between adjacent NRs was a few hundred nanometers). Therefore, the hydrogen bubbles attached to the top of the NRs, resulting in partially wetted NRs (Figure 4b). The excess hydrogen bubbles were arranged irregularly on the NRs and prevented a continuous gas interlayer from forming. Thus, the ZnO NR superhydrophobicity was only partially regenerated.

For the Si MPs with 50-μm pitches, ~ 70 % of the superhydrophobicity was recovered (Figure 4a). The regeneration of the superhydrophobicity was incomplete because the generated gas bubbles were isolated between the MP structures. The spacing between adjacent MPs was larger than the minimum gas bubble diameter of 20 μm, allowing stable hydrogen bubbles to form inside the Si MPs. Then, the gas bubbles gradually grew up the MP sides, almost reaching the top of the MPs.[32] Because the top of the MP was in contact with water, the separately grown gas bubbles could not coalesce to form a continuous gas overlayer (Figure 4c). Thus, the gas bubbles were isolated and remained between the MPs (Figure 4b), partially regenerating the superhydrophobicity. Complete regeneration of the underwater superhydrophobicity was only achieved with the ZnO/Si HRs (with ZnO NR length of 8 μm and Si MP pitches of 50 μm), as demonstrated by a final relative intensity of 100% for the PEC reaction (Figure 4a). During the PEC hydrogen generation, the spaces between the Si MPs were sufficient to allow hydrogen bubbles to form inside the MPs and prevent excess bubble formation on the surfaces. In addition, the ZnO NRs on the Si MPs retained the gas layer on the top of the Si MPs and served to unite the diffusing gas bubbles inside the Si MPs, which led to the formation of a continuous gas layer on the entire substrate. In contrast to the Si MP substrates, the gas bubbles formed between the MPs merged into a continuous gas layer on top of the HRs (Figure 4b). The regeneration of the gas layer was confirmed by microscope images (Figure 4c).

Developing a geometrical model for stably regenerating underwater superhydrophobicity

According to the experimental results, the optimized ZnO/Si HR geometry, including the MP spacing and NR length, was required to completely regenerate the underwater superhydrophobicity. For the bare MPs without ZnO NRs, although gas pockets were stably reformed between MPs with certain structural parameters according to the study of C. Lee *et al.*,[32] it was found that the MP structures were not sufficient for the formation of a continuous gas interlayer, as only 70% of the layer was regenerated. Thus, a modified model of the hierarchical ZnO NR/Si MP structures needed to completely regenerate the underwater superhydrophobicity was developed.

The modified equation, derived in Supplementary Information 6, defines the lower and upper bounds for stable regeneration of underwater superhydrophobicity.

$$\frac{\left(\sqrt{2}-2\sqrt{\frac{1-\phi}{\pi}}\right)\frac{-1+\sin\theta_p}{2\cos\theta_p}\times L-H}{\left(2\sqrt{2}-4\sqrt{\frac{1-\phi}{\pi}}\right)\frac{-1+\sin\theta_p}{2\cos\theta_p}+1}<d<\frac{\frac{-\cos\theta_b}{2\sin\theta_p(1-\sqrt{\pi(1-\phi)/\phi})}\times L-H}{\frac{-\cos\theta_b}{\sin\theta_p(1-\sqrt{\pi(1-\phi)/\phi})}+1}, \quad (1)$$

where L is bare Si MP pitch, H is bare Si MP height, d is ZnO NR length, ϕ is the gas fraction, and θ_p and θ_b are the water CAs of the ZnO NRs and the bottom surface between the MPs, respectively. This model gives the NR length (d) required to regenerate a stable gas interlayer in water and presents lower(d_{min})/upper(d_{max}) bounds, which are shown in Figure 5a. The water CA was fixed to 152° for the superhydrophobic ZnO NRs (θ_p) and to 114° for the hydrophobic Si MPs (θ_b).

Figure 5a shows those conditions in the plot of the NR length (d) vs the gas fraction (ϕ). The lower bound of d (d_{min}) in Figure 5a was derived from the minimum ZnO/Si HRs height/pitch ratio required to keep the water meniscus from contacting the bottom surface of the substrates. When MP pitch is 30 or 50 μm and MP height is 50 μm for

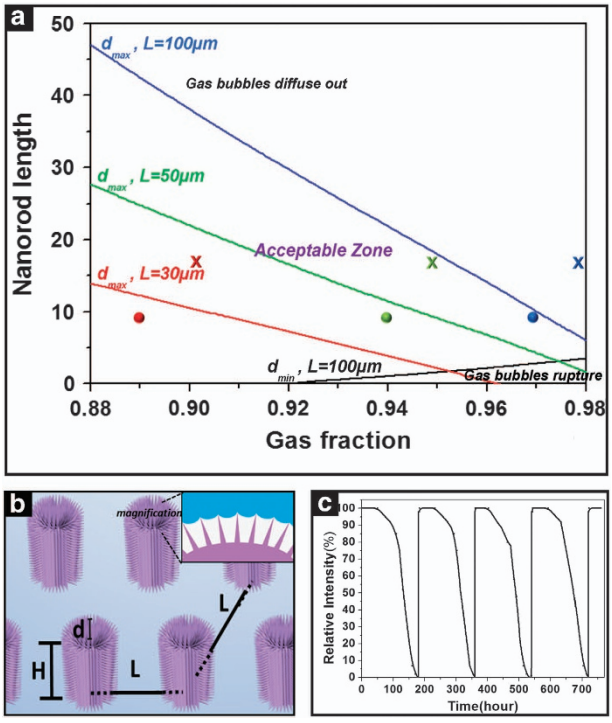

Figure 5 (**a**) Boundaries of the ZnO NR length required to allow gas bubbles to fill the interfacial region of the surface and form a stable gas interlayer theoretically calculated using equation (1). ● denotes the experimental results that involved the successful formation of a stable gas interlayer from the generated gas bubbles. All three ● data points are within the theoretically acceptable zone. **X** denotes the results of experiments in which a stable gas interlayer was not formed from the generated gas bubbles. All three **X** data points are outside the theoretically acceptable zone. (**b**) Three-dimensional schematic image of the ZnO/Si HRs. Inset image of **b** depicting magnified the ZnO NRs on top of the Si MPs in the ZnO/Si HRs. (**c**) Relative intensity transitions of the ZnO/Si HRs for several wetting and dewetting cycles.

the bare MPs, the d value is greater than the lower bound. The growth of ZnO NRs on the Si MPs results in an increase in the ZnO/Si HRs height/pitch ratio, and thus, d is always greater than the lower bound for the ZnO/Si HRs. However, when MP pitch is 100 μm and ϕ is greater than 0.9, it is possible that d might not be greater than the lower bound, which is plotted as a black line in Figure 5a. When the NR length is shorter than the lower bound, the generated gas bubbles cannot grow, and they rupture.

The upper bound of d (d_{max}) in the model was derived to ensure that the growth of the gas bubbles in the lateral direction is more favorable than that in the normal direction, meaning the lateral movements of the hydrogen bubbles are faster than the vertical movements. The upper bounds on d for MP pitch = 30, 50 and 100 μm are plotted as red, green and blue lines, respectively, in Figure 5a. The upper bound shifts upward as the pitch increases because a wider pitch allows the gas bubbles to spread along longer ZnO NRs. In addition, the pressure against lateral growth decreases with increasing pitch. When the ZnO NR length exceeds the upper bound, the gas bubbles do not grow laterally and instead escape from the surface due to decreased spacing between MPs. Depending on the MP pitch, the d values that allow gas bubbles to be captured and retained fall between d_{min} and d_{max}.

The ZnO/Si HRs experimental data collected for various NR lengths and MP pitches are included in Figure 5a to test the proposed model for regenerating underwater superhydrophobicity. When ZnO/Si HRs with a NR length of 8 μm and MP pitches of 30, 50 or 100 μm were used, the underwater superhydrophobicity was successfully regenerated, and, thus, the corresponding data points are marked with an **O**. They fall within the acceptable zone of the proposed model. By contrast, when ZnO/Si HRs with a longer NR length of 16 μm were employed, the underwater superhydrophobicity could not be regenerated, and, thus, the corresponding data points are marked with an **X**. These data points are located in the gas bubble diffusion zone (outside the acceptable zone for each MP pitch condition). These results demonstrate that the proposed model satisfactorily predicts the regeneration of underwater superhydrophobicity for the experimental conditions tested in this study. It should be noted that the ZnO NRs played a crucial role in forming a stable, continuous gas interlayer because the MP structure with no NRs had water on its surface, and the gas bubbles formed between each post could not merge to form a continuous gas layer. The ZnO NRs in the ZnO/Si HRs provided attachment points for the formation of a continuous gas interlayer, and the Laplace pressure of the ZnO NRs aided in the removal of the water layer on the surface (inset image of Figure 5b).[49] The details about Laplace pressure on the ZnO NRs are presented in the Supplementary Information 7.

Figure 5c shows the changes in the relative intensity for the superhydrophobic ZnO/Si HRs over five wetting (losing the gas interlayer) and dewetting (regenerating the gas interlayer) cycles. The wetting process required a few days due to the high stability of the underwater superhydrophobicity, whereas regeneration occurred within a few seconds. Reproducible trends and constant maximum intensity values were observed, meaning that the underwater superhydrophobicity was completely regenerated by the PEC reaction over several cycles. Also static water CAs of each state during the wetting–dewetting cycles were measured (Supplementary Figure S7). These results demonstrate the reproducibility of our regeneration method.

CONCLUSION

In summary, the lotus leaf effect (superhydrophobicity) and artificial leaf effect (solar water splitting) were combined for the first time to develop a method for completely regenerating the underwater superhydrophobicity of ZnO/Si hierarchical surfaces using photocatalytic hydrogen generation. The rationally designed n/p junction in the ZnO/Si HRs allowed for high gas interlayer stability in water as demonstrated by a long plastron lifetime and also highly reproducible regeneration of the underwater superhydrophobicity during cycling due to the unique ability of the surface to capture and retain a stable gas layer. A model was developed to define the optimal geometry of the surface structures for the formation of a stable, continuous gas interlayer on the superhydrophobic surface. The proposed model was consistent with our experimental results. This study presents a new possible solution to the continuing problem of the limited stability of underwater superhydrophobicity and broadens the applicability of superhydrophobic surfaces.

CONFLICT OF INTEREST

The authors declare no conflict of interest.

ACKNOWLEDGEMENTS

This work was supported by the National Research Foundation of Korea (2013-R1A2A2A05-005344).

1 Lafuma, A. & Quere, D. Superhydrophobic states. *Nat. Mater.* **2**, 457–460 (2003).
2 Feng, X. J. & Jiang, L. Design and creation of superwetting/antiwetting surfaces. *Adv. Mater.* **18**, 3063–3078 (2006).
3 Xia, D. Y., Johnson, L. M. & Lopez, G. P. Anisotropic wetting surfaces with one-dimesional and directional structures: fabrication approaches, wetting properties and potential applications. *Adv. Mater.* **24**, 1287–1302 (2012).
4 Deng, X., Mammen, L., Zhao, Y., Lellig, P., Müllen, K., Li, C., Butt, H. J. & Vollmer, D. Transparent, thermally stable and mechanically robust superhydrophobic surfaces made from porous silica capsules. *Adv. Mater.* **23**, 2962 (2011).
5 Zhou, H., Wang, H., Niu, H., Gestos, A., Wang, X. & Lin, T. Fluoroalkyl silane modified silicone rubber/nanoparticle composite: a super durable, robust superhydrophobic fabric coating. *Adv. Mater.* **24**, 2409–2412 (2012).
6 Zhao, Y., Qin, M. L., Wang, A. J. & Kim, D. Bioinspired superhydrophobic carbonaceous hairy microstructures with strong water adhesion and high gas retaining capability. *Adv. Mater.* **25**, 4561–4565 (2013).
7 Lai, Y. K., Pan, F., Xu, C., Fuchs, H. & Chi, L.F. *In situ* surface-modification-induced superhydrophobic patterns with reversible wettability and adhesion. *Adv. Mater.* **25**, 1682–1686 (2013).
8 Kim, S. B., Lee, W. W., Yi, J., Park, W. I., Kim, J. S. & Nichols, W. T. Simple, large-scale patterning of hydrophobic zno nanorod arrays. *ACS Appl. Mater. Inter.* **4**, 3910–3915 (2012).
9 Jung, Y. C. & Bhushan, B. Mechanically durable carbon nanotube-composite hierarchical structures with superhydrophobicity, self-cleaning, and low-drag. *ACS Nano* **3**, 4155–4163 (2009).
10 Park, K. C., Choi, H. J., Chang, C. H., Cohen, R. E., McKinley, G. H. & Barbastathis, G. Nanotextured silica surfaces with robust superhydrophobicity and omnidirectional broadband supertransmissivity. *ACS Nano* **6**, 3789–3799 (2012).
11 Pakdel, A., Bando, Y. & Golberg, D. Plasma-assisted interface engineering of boron nitride nanostructure films. *ACS Nano* **8**, 10631–10639 (2014).
12 Grewal, H. S., Cho, I. J., Oh, J. E. & Yoon, E. S. Effect of topography on the wetting of nanoscale patterns: experimental and modeling studies. *Nanoscale* **6**, 15321–15332 (2014).
13 Genua, A., Mecerreyes, D., Alduncín, J. A., Mondragon, I., Marcilla, R. & Grande, H.-J. Polymeric ionic liquids for the fast preparation of superhydrophobic coatings by the simultaneous spraying of oppositely charged polyelectrolytes and nanoparticles. *Polym J.* **43**, 966–970 (2011).
14 Nakajima, A. Design of hydrophobic surfaces for liquid droplet control. *NPG Asia Mater.* **3**, 49–56 (2011).
15 Hensel, R., Helbig, R., Aland, S., Voigt, A., Neinhuis, C. & Werner, C. Tunable nano-replication to explore the omniphobic characteristics of springtail skin. *NPG Asia Mater.* **5**, e37. doi:10.1038/am.2012.66 (2013).
16 Truesdell, R., Mammoli, A., Vorobieff, P., van Swol, F. & Brinker, C. J. Drag reduction on a patterned superhydrophobic surface. *Phys. Rev. Lett.* **97**, 044504 (2006).
17 Genzer, J. & Efimenko, K. Recent developments in superhydrophobic surfaces and their relevance to marine fouling: a review. *Biofouling* **22**, 339–360 (2006).

18 Lee, S., Lee, J., Park, J., Choi, Y. & Yong, K. Resistive switching WOx-Au core-shell nanowires with unexpected nonwetting stability even when submerged under water. *Adv. Mater.* **24**, 2418–2423 (2012).
19 Zhu, Q. & Pan, Q. M. Mussel-inspired direct immobilization of nanoparticles and application for oil-water separation. *ACS Nano* **8**, 1402–1409 (2014).
20 Liu, L., Yang, L. Q., Liang, H. W., Cong, H. P., Jiang, J. & Yu, S. H. Bio-inspired fabrication of hierarchical FeOOH nanostructure array films at the air-water interface, their hydrophobicity and application for water treatment. *ACS Nano* **7**, 1368–1378 (2013).
21 Chang, Y. H., Hau, N. Y., Liu, C., Huang, Y. T., Li, C. C., Shih, K. & Feng, S. P. A short-range ordered-disordered transition of a NiOOH/Ni(OH)(2) pair induces switchable wettability. *Nanoscale* **6**, 15309–15315 (2014).
22 Hiralal, P., Chien, C., Lal, N. N., Abeygunasekara, W., Kumar, A., Butt, H., Zhou, H., Unalan, H. E., Baumberg, J. J. & Amaratunga, G. A. Nanowire-based multifunctional antireflection coatings for solar cells. *Nanoscale* **6**, 14555–14562 (2014).
23 Gao, C., Sun, Z., Chen, Y., Li, K., Cao, Y., Zhanga, S. & Feng, L. Integrated oil separation and water purification by a double-layer TiO2-based mesh. *Energy Environ. Sci.* **6**, 1147–1151 (2013).
24 Zhang, L. B., Zhang, Z. H. & Wang, P. Smart surfaces with switchable superoleophilicity and superoleophobicity in aqueous media: toward controllable oil/water separation. *NPG Asia Mater.* **4**, e8. doi:10.1038/am.2012.14 (2012).
25 Zhu, Y. Z., Wang, D., Jiang, L. & Jin, J. Recent progress in developing advanced membranes for emulsified oil/water separation. *NPG Asia Mater.* **6**, e101. doi:10.1038/am.2014.23 (2014).
26 Poetes, R., Holtzmann, K., Franze, K. & Steiner, U. Metastable underwater superhydrophobicity. *Phys. Rev. Lett.* **105**, 166104 (2010).
27 Liu, W. D., Liu, X., Fangteng, J., Wang, S., Fang, L., Shen, H., Xiang, S., Sun, H. & Yang, B. Bioinspired polyethylene terephthalate nanocone arrays with underwater superoleophobicity and anti-bioadhesion properties. *Nanoscale* **6**, 13845–13853 (2014).
28 Maitra, T., Antonini, C., Auf der Mauer, M., Stamatopoulos, C., Tiwari, M. K. & Poulikakos, D. Hierarchically nanotextured surfaces maintaining superhydrophobicity under severely adverse conditions. *Nanoscale* **6**, 8710–8719 (2014).
29 Bobji, M. S., Kumar, S. V., Asthana, A. & Govardhan, R. N. Underwater sustainability of the 'cassie' state of wetting. *Langmuir* **25**, 12120–12126 (2009).
30 Marmur, A. Underwater superhydrophobicity: theoretical feasibility. *Langmuir* **22**, 1400–1402 (2006).
31 Lee, J. & Yong, K. Surface chemistry controlled superhydrophobic stability of W18O49 nanowire arrays submerged underwater. *J. Mater. Chem.* **22**, 20250–20256 (2012).
32 Lee, C. & Kim, C. J. Underwater restoration and retention of gases on superhydrophobic surfaces for drag reduction. *Phys. Rev. Lett.* **106**, 014502 (2011).
33 Li, Y., Li, L. & Sun, J. Q. Bioinspired self-healing superhydrophobic coatings. *Angew. Chem. Int. Ed.* **49**, 6129–6133 (2010).
34 Wang, H. X., Xue, Y., Ding, J., Feng, L., Wang, X. & Lin, T. Durable, self-healing superhydrophobic and superoleophobic surfaces from fluorinated-decyl polyhedral oligomeric silsesquioxane and hydrolyzed fluorinated alkyl silane. *Angew. Chem. Int. Ed.* **50**, 11433–11436 (2011).
35 Liu, Q. Z., Wang, X. L., Yu, B., Zhou, F. & Xue, Q. J. Self-healing surface hydrophobicity by consecutive release of hydrophobic molecules from mesoporous silica. *Langmuir* **28**, 5845–5849 (2012).
36 Zhu, D. D., Lu, X. M. & Lu, Q. H. Electrically conductive PEDOT coating with self-healing superhydrophobicity. *Langmuir* **30**, 4671–4677 (2014).
37 Walter, M. G., Warren, E. L., McKone, J. R., Boettcher, S. W., Mi, Q., Santori, E. A. & Lewis, N. S. Solar water splitting cells. *Chem. Rev.* **110**, 6446–6473 (2010).
38 Wolcott, A., Smith, W. A., Kuykendall, T. R., Zhao, Y. P. & Zhang, J. Z. Photoelectrochemical study of nanostructured ZnO thin films for hydrogen generation from water splitting. *Adv. Funct. Mater.* **19**, 1849–1856 (2009).
39 Seol, M., Kim, H., Kim, W. & Yong, K. Highly efficient photoelectrochemical hydrogen generation using a ZnO nanowire array and a CdSe/CdS co-sensitizer. *Electrochem. Commun.* **12**, 1416–1418 (2010).
40 Tak, Y. & Yong, K. J. Controlled growth of well-aligned ZnO nanorod array using a novel solution method. *J. Phys. Chem. B* **109**, 19263–19269 (2005).
41 Xia, Y. N. & Whitesides, G. M. Soft lithography. *Annu. Rev. Mater. Sci.* **28**, 153–184 (1998).
42 Zhang, Z., Chen, H., Zhong, J., Saraf, G. & Lu, Y. Fast and reversible Wettability transitions on ZnO nanostructures. *J. Electron. Mater.* **36**, 895–899 (2007).
43 Im, M., Im, H., Lee, J. H., Yoon, J. B. & Choi, Y. K. A robust superhydrophobic and superoleophobic surface with inverse-trapezoidal microstructures on a large transparent flexible substrate. *Soft Matter* **6**, 1401–1404 (2010).
44 Larmour, I. A., Bell, S. E. J. & Saunders, G. C. Remarkably simple fabrication of superhydrophobic surfaces using electroless galvanic deposition. *Angew. Chem. Int. Ed. Engl* **46**, 1710–1712 (2007).
45 Xue, Y.H., Chu, S.G., Lv, P.Y. & Duan, H.L. Importance of hierarchical structures in wetting stability on submersed superhydrophobic surfaces. *Langmuir* **28**, 9440–9450 (2012).
46 Kargar, A., Sun, K., Jing, Y., Choi, C., Jeong, H., Zhou, Y., Madsen, K., Naughton, P., Jin, S., Jung, G. Y. & Wang, D. Tailoring n-ZnO/p-Si branched nanowire heterostructures for selective photoelectrochemical water oxidation or reduction. *Nano Lett.* **13**, 3017–3022 (2013).
47 Ljunggren, S. & Eriksson, J. C. The lifetime of a colloid-sized gas bubble in water and the cause of the hydrophobic attraction. *Colloid Surface A* **129**, 151–155 (1997).
48 Liebermann, L. Air bubbles in water. *J. Appl. Phys.* **28**, 205 (1957).
49 Wang, J. M., Zheng, Y. M., Nie, F. Q., Zhai, J. & Jiang, L. Air bubble bursting effect of lotus leaf. *Langmuir* **25**, 14129–14134 (2009).

Supplementary Information accompanies the paper on the NPG Asia Materials website (http://www.nature.com/am)